Liquid Crystals
Publication details, including instructions for authors and subscription information:
http://www.informaworld.com/smpp/title~content=t713926090

Permeative flow and the compatability of smectic C zig-zag defects with compressive and dilative regions

M. J. Towler; D. C. Ulrich; I. W. Stewart; H. G. Walton; P. Gass

Online publication date: 06 August 2010

To cite this Article Towler, M. J. , Ulrich, D. C. , Stewart, I. W. , Walton, H. G. and Gass, P.(2000) 'Permeative flow and the compatability of smectic C zig-zag defects with compressive and dilative regions', Liquid Crystals, 27: 1, 75 — 80
To link to this Article: DOI: 10.1080/026782900203245
URL: http://dx.doi.org/10.1080/026782900203245

LIQUID CRYSTALS, 2000, VOL. 27, NO. 1, 75–80

Permeative flow and the compatability of smectic C zig-zag defects with compressive and dilative regions

M. J. TOWLER, D. C. ULRICH, I. W. STEWART†, H. G. WALTON* and P. GASS

Sharp Laboratories of Europe Ltd, Oxford Science Park, Oxford OX4 4GA, UK
†Department of Mathematics, University of Strathclyde, Glasgow G1 1XH, UK

(*Received 16 June 1999; accepted 2 August 1999*)

Mukai and Nakagawa have predicted that hairpin and lightning defects correspond to compressive and dilative regions in the smetic C layer structure. Walton *et al.* have previously used the Helfrich–Hurault effect and an induced SmA–SmC phase transition to reconfirm the existence of such dilated and compressed regions under situations of permeative flow. In the present work, flow-induced compression and dilation is used to confirm the first prediction. Situations of asymmetric zig-zag defect generation are observed and some possible explanations offered. Situations in which flow is induced by mechanical cell deformation, and where electric field-induced director switching leads to material pumping are also discussed.

1. Introduction and theoretical background

The one-dimensional layered nature of smectic liquid crystals has dramatic consequences for the hydrodynamic behaviour of these systems. Hydrodynamic flows can couple to pressure gradients, leading to layer distortions and the appearance of sample defects. Flow studies can yield improved understanding of the physical properties of these phases and have practical relevance in the design of stable, defect-free display devices.

The liquid-like flow within smectic layers is described by a Navier–Stokes-like equation, whilst the permeative flow across the layers is described by Darcy's law [1–5]. Previously, Walton *et al.* [6] considered flow in the SmA and SmC phases past a finite rigid barrier of unit length centred at the origin in the *xz*-plane and lying along the vertical *z*-axis (figure 1). The bookshelf smectic layers run perpendicular to the barrier, but parallel to the direction of induced flow in the horizontal *x*-direction. By considering only the velocity components v_x and v_z in the *xz*-plane the governing dynamic equations reduce to

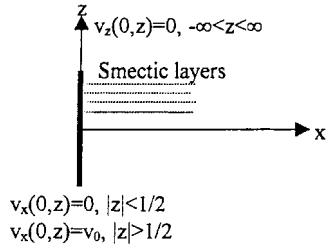

Figure 1. Schematic view coordinate system with finite barrier of unit length centred at the origin in the *xz*-plane.

* Author for correspondence; e-mail: harryw@sharp.co.uk

$$\frac{\partial P}{\partial z} = \frac{-v_z}{\lambda_p} \tag{1a}$$

$$\frac{\partial P}{\partial x} = \eta_3 \frac{\partial^2 v_x}{\partial z^2} \tag{1b}$$

$$\frac{\partial v_x}{\partial x} + \frac{\partial v_z}{\partial z} = 0 \tag{1c}$$

where P is the applied pressure, λ_p is the permeation coefficient and η_3 is a viscosity coefficient. The boundary conditions are

$$v_x(0, z) = 0, |z| < \frac{1}{2}; v_x(0, z) = v_0, |z| > \frac{1}{2} \tag{2}$$

$$v_z(0, z) = 0, -\infty < z < \infty . \tag{3}$$

The analtyic solution for the flow velocity components was previously shown [6] to be:

$$v_x = v_0 - \frac{v_0}{2}\{\mathrm{erf}[(z + 1/2)/2\sqrt{(\delta|x|)}] - \mathrm{erf}[(z - 1/2)/2\sqrt{(\delta|x|)}]\} \tag{4}$$

$$v_z = \pm \frac{v_0 \delta^{1/2}}{\sqrt{\pi|x|}} \sinh(z/4\delta|x|) \exp[-(z^2 + 1/4)/4\delta|x|] \tag{5}$$

where erf is the usual error function and v_0 is the magnitude of the flow velocity in the *x*-direction at

infinity. The parameter $\delta = \sqrt{\lambda_p \eta_3}$ has units of length and sets a scale for boundary layer phenomena. v_x is taken as positive for $x < 0$ and negative for $x > 0$. For $x > 0$, the maximum magnitude of v_z occurs when

$$x = \frac{z}{2\delta \ln\left(\dfrac{2z+1}{2z-1}\right)}. \tag{6}$$

In order to follow the behaviour of the smectic layer displacement u (and more particularly $\partial u/\partial z$) and hence image the compressive and dilative regions of the system, we relate layer displacement to applied pressure P through the introduction of a layer compressional elastic constant B in equation (1 *a*) [4]:

$$\partial u/\partial z = BP \tag{7}$$

giving

$$\frac{-v_z}{\lambda_p B} = \frac{\partial^2 u}{\partial z^2}. \tag{8}$$

We consider a cell that is finite, but large ($L \gg 1$) in the z-direction; then u must satisfy the boundary conditions

$$u(x, -L) = u(x, 0) = u(x, L). \tag{9}$$

Equations (8) and (9) lead to

$$B\lambda_p u = -\int_{-L}^{z}\int_{-L}^{z_2} v_z(x, z_1)\,dz_1\,dz_2 + \frac{L+z}{2L}\int_{-L}^{L}\int_{-L}^{z_2} v_z(x, z_1)\,dz_1\,dz_2 \tag{10}$$

and the change in layer displacement as z varies is derived from

$$B\lambda_p \frac{\partial u}{\partial z} = -\int_{-L}^{z_2} v_z(x, z_1)\,dz_1 + \frac{1}{2L}\int_{-L}^{L}\int_{-L}^{z_2} v_z(x, z_1)\,dz_1\,dz_2. \tag{11}$$

Figure 3 shows the typical qualitative behaviour of u and $\partial u/\partial z$ when $L = 50$ and, for simplicity, both $B\lambda_p$ and v_0 are set to unity and the parameter δ is set equal to 0.5. Rescaling $B\lambda_p$ simply rescales the amplitude of u, whilst changes to L have only small effects due to the exponential nature of equation (5). Figure 3 (*b*) shows $\partial u/\partial z$ for $|z| \leqslant 3$ for the indicated values of x. It is evident that $\partial u/\partial z$ has its greatest rate of change when $\partial^2 u/\partial z^2$ is at a maximum. From equations (5) and (7) this maximum occurs along the lines provided by equation (6), which are shown as the inner pair of lines in figure 2. Figure 3 (*c*) shows contours of constant $\partial u/\partial z$ (i.e. constant compression/dilation) behind the barrier centred at $x = 0$.

2. Experimental observations and discussion

A 3 μm thick, parallel rubbed polyimide cell was fabricated with a photolithographically produced 50 μm diameter pillar at its centre and filled with the commercial material SCE8 (Cr < − 20 SmC 58 SmA 78 N* 98 I, °C). The cell thickness was decreased at a far (negative) distance from the pillar and the consequences of the resultant flow past the obstacle were observed at different temperatures, both in the SmA phase and the SmC phase.

2.1. *Smectic A*

Smectic A layers subjected to a dilation undergo a buckling instability [7] above a threshold which remains finite at all temperatures. Layers subjected to compression undergo a SmA to SmC phase transition (i.e. induced tilt) above some threshold stress. The threshold for induced tilt is large for above T_{AC} but tends to zero as the second order phase transition is approached [7]. The buckling instability was previously used by Clark [8] to confirm the existence of dilated regions when flow occurred past an air bubble in a cell filled with a liquid crystal in the SmA phase. In [6] we were able to reconfirm this observation for the SmA phase, and by

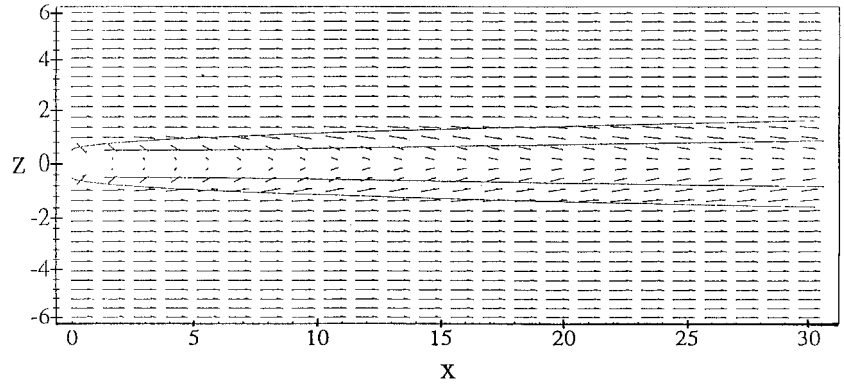

Figure 2. Calculated flow profile after the barrier. Outer lines show a parabolic-type boundary layer, outside of which the z-component of flow becomes small; inner lines show the condition for maximum z-component of velocity.

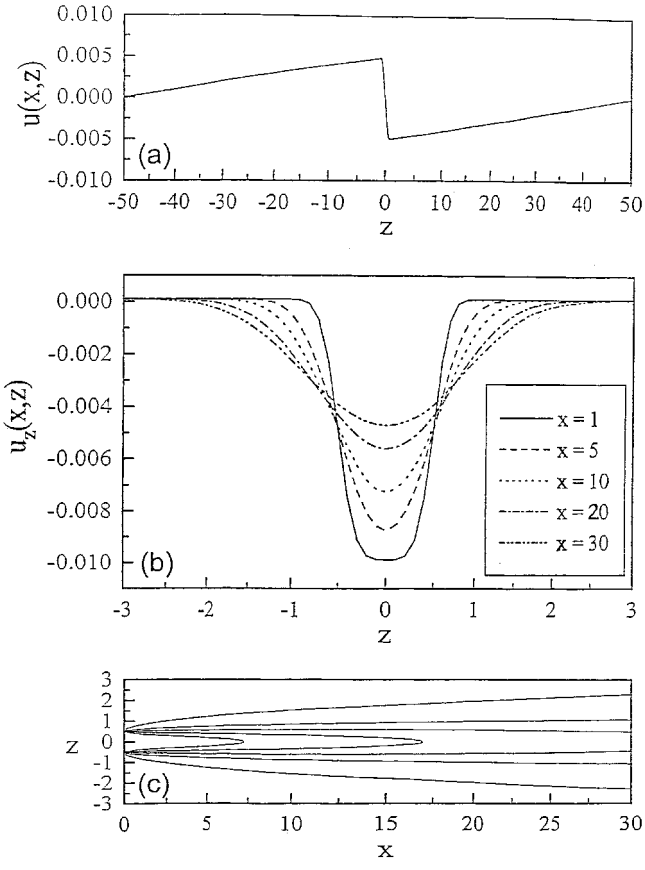

Figure 3. (*a*) Form of u (c.f. equation (9)) for $x = 1$; (*b*) shows $\partial u/\partial z$ (c.f. equation (10)) for $z < 3$ for indicated values of x; (*c*) is a contour plot of $\partial u/\partial z$. The outer curves are for $\partial u/\partial z = 0$ and (working inwards) the contours represent $\partial u/\partial z = -0.002$, -0.004, -0.006 and -0.008, respectively.

holding the sample at a temperature close to SmC, were also able to image the regions of compression via the induced director tilt and the accompanying changes in birefringence. Indeed, very close (~ 0.1°C) to the SmC, it proved unnecessary to induce flow manually in the sample to observe compression, since small random flows driven by minor temperature fluctuations were sufficient to induce considerable fluctuations in birefringence in line with the barrier.

It is of interest to note that the threshold for layer buckling depends inversely upon sample extension along the layer normal. In principle therefore, an infinitesimal dilative force, acting anywhere in the (effectively) infinite (~ 1 cm) region of sample outside the line of the barrier would seem sufficient to result in layer buckling [4]. As noted in [6] however, at very low flow rates in the SmA, we do not observe dilative buckling. Whether buckling is present, but on a scale insufficient to scatter light strongly, or whether the finite cell thickness ($\sim$ μm) rescales the threshold for the instability is currently unclear.

Nevertheless, theoretically the shape and location (though not the absolute threshold) of the observed regions of sample buckling and induced tilt can be well understood by comparison with figures 2 and 3. The $v_z(z) = -v_z(-z)$ symmetry and the related behaviour of $\partial u/\partial z$ are reflected in the experimental observations. Experimentally the symmetry of $v_z(z)$ is clearly observed as flow alignment (hence flow birefringence) of the induced SmC domains.

2.2. *Smectic C*

It is well known that thin planar samples of SmC can form a chevron layer structure, with two (untwisted) chevron types possible ('C1' and 'C2') characterized in part by differing signs of layer tilt. In some situations (for example, with low surface pretilt), regions of both C1 and C2 can form within a sample with the boundary between the regions highlighted by a characteristic

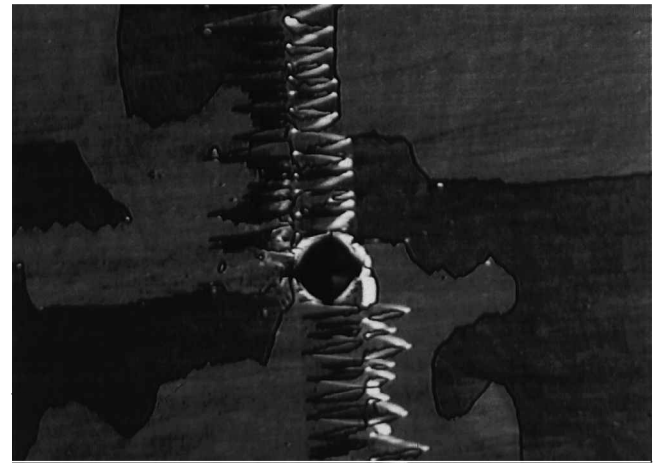

(*a*)

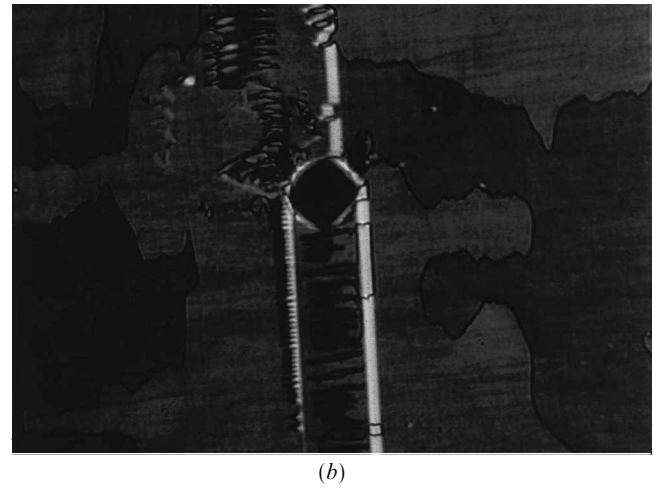

(*b*)

Figure 4. Response of SmC C2 chevron state at $T - T_{AC} = -33$°C to a bottom-to-top flow past a cylindrical barrier: (*a*) low flow rate, (*b*) high flow rate.

zig-zag defect possessing a broad 'hairpin' section and a thinner 'lightning' section. Although not relating their discussion to flow, Mukai and Nakagawa [9] have shown that the hairpin and lightning zig-zag defect structures are, respectively, compatible with compressive and dilative layer geometries in the SmC. Strictly, the theoretical derivation of the velocity fields and layer displacements given previously is valid only for bookshelf SmA before the onset of layer distortions. Nevertheless it allows us to make some qualitative predictions for flow in the chevron SmC. Following [9] we can expect the creation of hairpin defects in compressed SmC regions and lightning defects in dilated regions.

Figure 4 (*a*) shows the effect of flow in a cell initially uniformly aligned in the C2 state and held at a temperature $T_{AC} - T = 33°C$. A clearly asymmetric defect pattern is observed. Before the barrier a lightning defect (darker line) is formed in the dilated region as expected; however a hairpin defect (thicker, white line) forms in only one of the compressed regions (to the right of the barrier as viewed in the photomicrograph). A similar behaviour is observed after the barrier. It is observed that at higher flow velocities some symmetry is restored, figure 4 (*b*); the hairpin defect (though of reduced lateral extent), forms in both of the compressed regions before the barrier.

We suggest that the initial asymmetry of defect formation at low flow rate and later symmetry restoration at higher flows can be understood from the constraint that in the uniform C2 cell the formation of a hairpin defect (i.e. a flip to the C1 state) at one position in the sample must necessarily be accompanied by the formation of a lightning defect elsewhere, in order for the sample to return to the equilibrium C2 state at large distances (see figure 5). If we consider the region before a barrier in a sample, by analogy with the SmA we expect a central region of dilation to result from flow past the barrier, with two regions of compression on either side. Formation of a hairpin/lightning pair allows the stress in the central dilated region and one of the adjacent compressed regions to be relaxed. Formation of a second hairpin wall would help to relax the stress in the second compressed region, but the necessary formation of a paired lightning wall would then have to occur some distance from the barrier, with no dilative force present to aid its formation. Only for sufficiently large flows is it favourable for the system to respond in both regions of compression by forming hairpin walls at the cost of elsewhere nucleating a lightning defect in a non-dilated region. A theoretical exposition of this argument would require a compressible SmC model and evaluation of defect wall energies. We have not attempted these calculations.

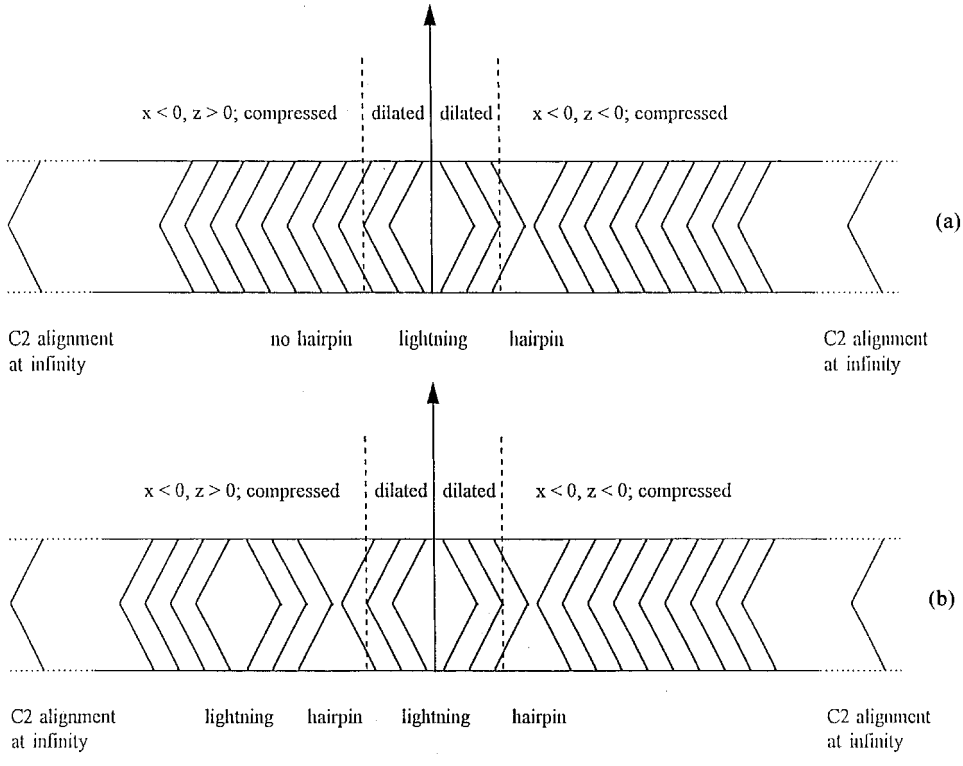

Figure 5. Schematic cross section of layer structure with $x < 0$: (*a*) corresponds to figure 4 (*a*); (*b*) corresponds to figure 4 (*b*).

Although our qualitative model appears to describe the observations, we also note here that in principle the asymmetric nature of the chevron structure could lead to other asymmetric behaviours close to a barrier. For example, material flowing along x and reaching the barrier at point 'a' in figure 6, may acquire a non-zero v_y to enable it to pass the barrier and continue along the x-direction at point 'b'. The situation is asymmetric

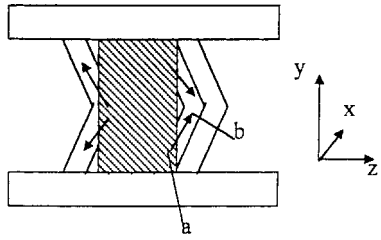

Figure 6. Schematic showing possibility of induced v_y for tilted layer geometries.

either side of the barrier, as indicated by the arrows. Given the relative magnitudes of the pillar (50 μm diameter), cell thickness (~ 3 μm) and layer tilt angle (~ 15°–20°), this effect may however be small.

2.3. *Smectic C*: pumping-induced flow*

Berreman [10] has demonstrated that electric field-induced director switching can induce flow in liquid crystals. Jakli and Saupe [11] and Zou *et al.* [12] have shown that asymmetric a.c. switching voltages can induce unidirectional flow in a SmC* sample, with the direction of flow depending upon the polarisation ($\mathbf{P}_s$) state of the sample and the asymmetry arising from director reorientation around the cone. We have been able to induce flow past a 50 μm pillar in a cell by the application of a cyclic waveform comprising a 22.5 μs bipolar pulse with 80 $V_{p\text{-}p}$ amplitude (leading pulse positive) followed by a 3 ms, 0 V period. Asymmetric

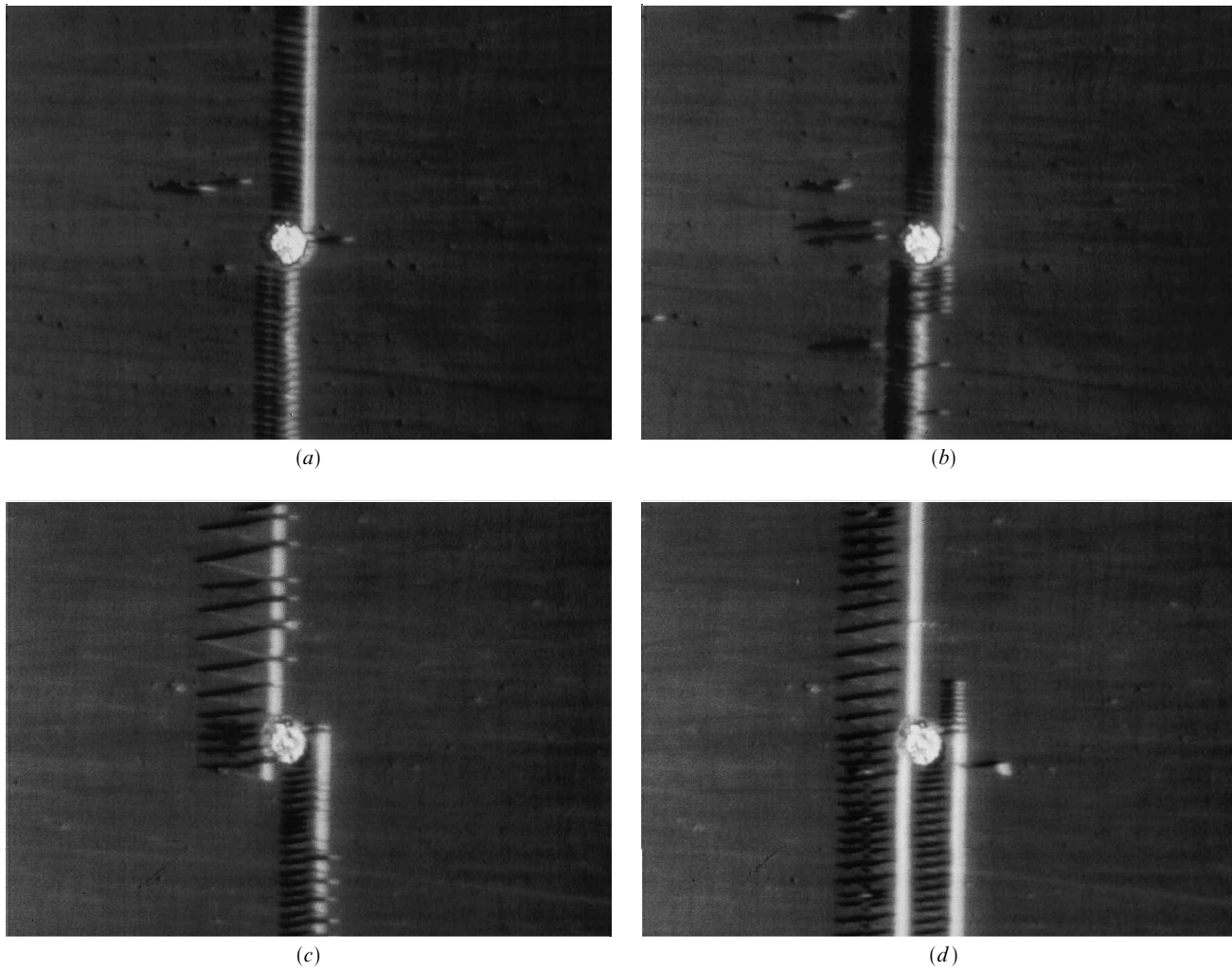

(*a*) (*b*)

(*c*) (*d*)

Figure 7. Electrical pumping induced flow. (*a*) From top-to-bottom, low flow rate; (*b*) top-to-bottom, higher flow rate; (*c*) bottom-to-top, low flow rate; (*d*) bottom-to-top, higher flow rate.

switching (and hence flow) results, since the leading positive pulse acts on a relaxed director structure, whilst the trailing negative pulse acts on an elastically stressed director state. By analogy with the situation described in the previous section, we can expect the asymmetric formation of zig-zag defects below some flow rate, whilst at high flow rates the pressure gradients can become sufficiently large to restore some symmetry to the zig-zag structure despite the requirement for additional layer distortions. In practice we observe asymmetric zig-zag formation when the bipolar pulse width is 22.5 μs figure 7 (*a*). Symmetry is restored when the pulse width is increased to 30 μs, with the lightning regions appearing in both dilative regions after the barrier, at the expense of forming a hairpin defect to one side, figure 7 (*b*).

When the asymmetry of the driving signal is reversed, the pumping direction also changes. Initially the defect pattern forms asymmetrically, figure 7 (*c*), opposite to that of figure 7 (*a*). Once the waveform has been continuously applied for ~ 1 min some symmetry is restored as a hairpin defect forms in both compressed regions before the barrier. Further symmetry is seen as a lightning defect begins to form in the right-most dilative region after the barrier, once again at the expense of forming an additional hairpin, figure 7 (*d*).

3. Conclusion

We have extended the analysis of [6] to enable the calculation of the pre-instability layer displacement field induced by flow past a finite barrier in the SmA phase. Both the expected regions of dilation and compression have been confirmed in the SmA phase by observing the Helfrich–Hurault instability and the SmA–SmC phase transition. These flow-induced regions of dilation and compression have been used to confirm the prediction of [9], namely that in thin chevron SmC samples, the hairpin zig-zag defect is compatible with regions of compression and the lightning zig-zag defect is compatible with regions of dilation. Various symmetries of the defect formation are observed in the vicinity of the barrier in the cells. We have proposed a qualitative model to account for these observations.

Observations of the unusual hydrodynamic symmetries of smectic liquid crystals offer opportunities for improved understanding of these phases. More detailed experiments can be expected to yield improved values of permeation coefficients, compressional elastic constants and the threshold energies and mechanisms of smectic defect formation. We can expect improved understanding to be of both fundamental interest and of practical utility for the construction of defect-free and damage-resistant smectic liquid crystal devices, where flow (electrically pumped or otherwise) past obstacles can result in image degradation.

References

[1] Helfrich, W., 1969, *Phys. Rev. Lett.*, **23,** 373.
[2] Martin, P. C., Parodi, O., and Pershan, P. S., 1972, *Phys. Rev. A*, **6,** 2401.
[3] Landau, L. D., and Lifschitz, E. M., 1986, *Theory of Elasticity*, 3rd Edn (Oxford: Oxford University Press).
[4] De Gennes, P. G., and Prost, J., 1993, *The Physics of Liquid Crystals*, (Pergamon) 2nd Edn (Pergamon), p. 443.
[5] De Gennes, P. G., 1974, *Phys. Fluid.*, **17,** 9.
[6] Walton, H. G., Stewart, I. W., and Towler, M. J., 1996, *Liq. Cryst.*, **20,** 665.
[7] Ribotta, R., and Durand, G., 1977, *J. Physique*, **38,** 179.
[8] Clark, N. A., 1978, *Phys. Rev. Lett.*, **40,** 1663.
[9] Mukai, S., and Nakagawa, M., 1994, *Jpn. J. appl. Phys.*, **33,** 6255.
[10] Berreman, D. W., 1979, *J. appl. Phys.*, **50,** 8016.
[11] Jakli, A., and Saupe, A., 1991, *Liq. Cryst.*, **9,** 519.
[12] Zou, Z., Clark, N. A., and Carlsson, T., 1994, *Phys. Rev. E.*, **49,** 3021.